criteria based on phenomenological continuum dynamics. In failure criteria based on equivalent plastic strain, $\bar{\varepsilon_p}$, formulation of equivalent plastic strain is given as

$$\bar{\varepsilon_p} = \frac{\sqrt{2}}{3}[(\varepsilon_1 - \varepsilon_2)^2 + (\varepsilon_2 - \varepsilon_3)^2 + (\varepsilon_3 - \varepsilon_1)^2] \quad \text{(Eq. 2.1)}$$

Bohl and Butler used that failure occurred within 12% of equivalent plastic strain while Berman placed the criterion of 18%. For metallographic rupture, failure occurs for following case,

$$\varepsilon_{pg} \leq \varepsilon_{pmax} \quad \text{(Eq. 2.2)}$$

$\varepsilon_{p\max}$ is maximum principal plastic strain, ε_{pg} is failure plastic stain and failure plastic strain is obtained from following formulation.

$$\varepsilon_{pg} = 126.1\left[\frac{1+\beta^2-1.2\beta}{1+\beta}\right](1+\delta^2+1.2\delta)^{-0.5} \quad \text{(Eq. 2.3)}$$

β and α are defined as

$$\beta = \frac{1.5+2.5\delta}{2.5+2.5\delta}, \ \delta = \frac{\varepsilon_1}{\varepsilon_2} \quad \text{(Eq. 2.4)}$$

If this criterion is applied, failure occurs at same location but failure reaction is slightly delayed compared to 12% or 18% criteria mentioned above. Failure criteria for ductile material are generally based on plastic equivalent strains and ranges from 13% to 18% are conservative [Reference 11].

Shockey [Reference 28] adopted concept of ductile fracture apparatus based on void generation and growth. He found that void was generated from precipitation particle and critical strain required for void nucleus generation is 11%. This is also modification of maximum tensile strength that corresponds to beginning of necking. Bang [Reference 25] used this design criterion for the evaluation of the KNGR reactor vessel integrity against IVSE loads estimated by the TRACER code [Reference 29].

Recently, Corradini et al., [Reference 30] evaluated the vessel integrity of a new design reactor, NuScale PWR. They modeled the RPV wall by an elastic-plastic deformation model to determine the failure threshold for the dynamic pressure loads with a given peak-pressure and pulse width. By assuming the stress is constant (and equal to the yield stress), they modeled the shell by the following second order differential equation:

$$\frac{d^2y}{dt^2} = \frac{(rP - 2t\sigma)}{rt\rho} \quad \text{(Eq. 2.5)}$$

where y is the radial displacement, P is the internal pressure, r is the mean radius of the shell, t is the shell wall thickness, σ is the yield stress of the shell material, and ρ is the density of the shell material. In this model, they assumed that significant yielding occurred in the solid and the material

was perfectly plastic. They assumed that the failure occurred a hoop strain limit of 50%, reduced by a factor of 2.25 to account for biaxiality effects. In summary, for the failure criterion of the APR1400 RPV against IVSE loads, the Shockey criterion is selected for the conservatism.

It is assumed that the boundary pressure loading on the RPV inner wall be the maximum pressure pulse calculated by the TEXAS-V code over the entire inner wall boundary without the consideration of the pressure attenuation while travelling from the location of the explosion to the wall for the conservatism standpoint. ABAQUS 6.10 is used for stress analysis FEM tool. To apply real time to stress analysis, explicit mode of ABAQUS is used.

2.2.2. Ex-Vessel Steam Explosion (EVSE)

EVSE occurs when RPV failed due to the lack of adequate cooling of the corium relocated to the lower plenum in the vessel while water is available outside the reactor vessel. For the EVSE analysis, it is necessary to know the thermal conditions of corium at the time of vessel failure such as corium composition for the thermo-physical properties, corium temperature etc., the modes of vessel failure that include the vessel failure location, size and corium ejection velocity and the conditions of cavity environment that includes the thermal conditions of water, ambient pressure and flooded water heights. Those parameters are considered as initial and boundary conditions that strongly depend on the accident sequences and scenarios. Therefore for the adequate definition of the conditions, it is required that rigorous accident analyses should be performed. For the reason, information to characterize the corium flow in EVSE are obtained from accident system code analysis for the corium formation in RPV such as the SCDAP/RELAP5, and MAAP analysis results [Reference 31, 32] as well as experimental evidences available in literatures and separate studies will be used as the initial and boundary conditions for EVSE.

TEXAS-V is also employed as an analysis tool to evaluate the EVSE energetics. As described in the previous section, the one-dimensional code will provide a conservative estimation for the given EVSE specific conditions. In particular for the estimation of explosion pressure on the cavity wall that is located at a distance away from the potential steam explosion interaction zone, underwater pressure attenuation should be considered.

2.3. Description of the TEXAS-V Code

TEXAS is a mechanistic model used for FCI analysis. The following is a brief description of the TEXAS models relevant to quenching calculations. It is essentially a condensed version of the description of the TEXAS model from Chu's and Tang's PhD thesis [Reference 33, 34].

The original TEXAS code was a parametric model developed by Young [Reference 35] for the design and analysis of fuel-coolant interaction experiments for LMFBR safety related issues. In an attempt to extend the capabilities of TEXAS, Chu and Corradini [Reference 36] incorporated a dynamic fragmentation model and a complete set of constitutive correlation's for interfacial mass, momentum, and energy transport terms; i.e., TEXAS-II. Since then, several improvements to the explosion propagation modeling, in particular, have been introduced by Tang [Reference 34]. A chemical reaction model to account the heat generation by oxidation of metallic melt was added by Murphy [Reference 17]. These updates warranted a new release of the model, TEXAS.

The TEXAS code is a transient, three fluid, one-dimensional model capable of simulating fuel-coolant mixing interactions. The three fields include two Eulerian fields for coolant liquid and vapor, and one Lagrangian field for fuel particles. The multifield feature of the code allows it to model thermal and mechanical nonequilibrium between coolant liquid and vapor which is very likely the case for fuel-coolant interactions. The code has the ability to handle flow regime transitions, which is also important to realistically model the heat transfer process. The "Lagrangian" treatment for the fuel field makes it easier to track the fuel particle movement, and eliminates some numerical difficulties encountered in pure Eulerian codes. The fragmentation model used in the code is based on hydrodynamic instabilities (i.e., Rayleigh-Taylor). The code also provides choices of velocity, pressure, and reflective (or closed) boundary conditions, giving more flexibility to users in different applications. A semi-implicit numerical technique is used in TEXAS which is a modified version of the SIMMER-II method, the actual forerunner of the TEXAS hydrodynamic formulation. With this method, the pressure iteration is done in a loop in which the energy and momentum equations are solved semi-implicitly, whereas the continuity equations are solved implicitly by adjusting the pressure distribution such that the errors of the continuity equations for all cells are reduced to a given tolerance. The Newton-Raphson method is employed in this pressure iteration.

2.3.1. Steam Explosion Models: Fragmentation Models

The key constitutive relation in TEXAS-V is the hydrodynamic fuel fragmentation model. This model was developed by Chu and Corradini [Reference 36] based on Pilch's original concept [Reference 37] of a multi-step fragmentation theory for liquid particles. The model considers the fuel particles to be deformed and dynamically fragmented into a discrete number of particles from its initial diameter to smaller sizes. The fragmentation mechanism assumed in the model is Rayleigh-Taylor instabilities. The shear forces caused by the parallel velocity (e.g., Kelvin-Helmholtz instabilities and boundary layer stripping) are neglected because of their limited effects with a vapor film present. The correlation of this theoretical model reads as:

$$D(T^+) = D(0)\exp[-C_1(T^+)^{C_2}We^{C_3}] \quad \text{(Eq. 2.6)}$$

By averaging the fragmentation rate, the above equation can be simplified to a linear time-independent form, which is used in TEXAS-V:

$$D_f^{n+1} = D_f^n\left(1 - C_0\Delta T^+ We_e^{1/4}\right) \quad \text{(Eq. 2.7)}$$

where the superscripts *n,n+1* designate old and new time step values; *We* is the Weber number for the fuel particles; T^+ is a dimensionless time step; and C_O is the constant:

$$We = \frac{\rho_c U_r^2 D_f^n}{\sigma_f} \quad \text{(Eq. 2.8)}$$

$$\Delta T^+ = \frac{U_r(t^{n+1} - t^n)}{D_f^n}\left(\frac{\rho_c}{\rho_f}\right)^{1/2} \quad \text{(Eq. 2.9)}$$

$$C_0 = 0.1093 - 0.0785\left(\frac{\rho_c}{\rho_f}\right)^{1/2} \quad \text{(Eq. 2.10)}$$

where U_r is the relative velocity; D is the fuel diameter: and ρ_f and ρ_c is the densities of fuel and coolant.

The conceptual model based on Corradini and Kim's model [Reference38] as shown in Figure 2-1 was employed in the TEXAS code in a semi-empirical relationship as shown in Eq. (2.12) depicting the fine fragmentation rate is proportional to the micro liquid jet velocity generated by the Rayleigh-Taylor instabilities and a function of fine fragmentation rate.

$$\dot{m}_{fr} \sim u_j F(t_f)$$
$$u_j = \left(\frac{\Delta P}{\rho_c}\right)^{0.5} \quad \text{(Eq. 2.11)}$$

The final expression for the fine fragmentation becomes

$$\dot{m}_{fr} = 6C_{fr}m_p\left(\frac{P - P_{th}}{\rho_f D_p^2}\right)^{0.5} F(\alpha)g(\tau) \quad \text{(Eq. 2.12)}$$

Here, the fine fragmentation rates depend strongly on local pressure, mixing particle diameter and model parameters such as the fragmentation coefficient, C_{fr} and the local phase factor, F. In this analysis, C_{fr} of 0.002 was used, since the value was well evaluated with experimental data [Reference 39]. Local void fraction of 0.3 is used for the threshold value for the F factor, meaning the fine fragmentation process terminated at the local void fraction of 0.3. The threshold pressure of vapor film collapse surrounding melt particles, P_{tr}, is set to 0.2 MPa. The function, $g(\tau)$ is a characteristic time function which is defined by

$$g(\tau) = \begin{cases} 1 & \text{for } \tau < \tau_c \\ 0 & \text{for } \tau > \tau_c \end{cases}, \quad \text{(Eq. 2.8)}$$

where τ_c is the characteristic time for fine fragmentation and is given to 2~4 ms as observed in single drop experiments [Reference 40].

The TEXAS-V model does not consider all the processes that may occur during melt jet mixing or the explosion phase. A key empirical observation from the KROTOS and FARO tests is that energetics with molten corium is substantially reduced from what had been observed with simulants (e.g., aluminum oxide).

Although this has been empirically seen in a number of experiments, there is still no clear reason for this observation. One possible explanation is that the corium partially solidifies and develops a solid 'skin' resisting rapid fuel fragmentation. No FCI model has the ability to locally model the effects of fuel partial solidification within a large collection of fuel drops in the coolant. This large reduction in energetics is not considered in these analyses, to be conservative, but is the focus of current modeling that briefly discussed in the next section.

2.3.2. New TEXAS Code: TEXAS-VI

Chen and Corradini [Reference 7] recently upgrade the TEXAS code, denoting the new TEXAS model as TEXAS-VI, by employing the fuel particle solidification model and solidifying fuel particle fragmentation criteria based on thermal stress and the modified Aeroelastic number. The new model has been verified with the FARO test, L14, and OECD standard problem [Reference 5] for FCI analysis.

This implementation is able to take account of the material solidification issues to examine the lower steam explosion energetics associated with the low superheat corium. In this model, the corium is considered as totally opaque for thermal radiation and the energy balance for fuel particle is formatted by heat conduction. The criterion of fragmentation for solidifying particle was set in terms of the modified Aeroelastic number and thermal stress.

The validation results with the FARO-L14 test demonstrated the effect of solidification on the mixing phase of steam explosion, especially for jet breakup, showing the good agreement of the L14 experiment data and also the slower increase of the fuel surface area prediction than one by TEXAS-V due to the limited rapid fragmentation. No validation efforts of the TEXAS-VI code for the explosion phase of steam explosion have been reported.

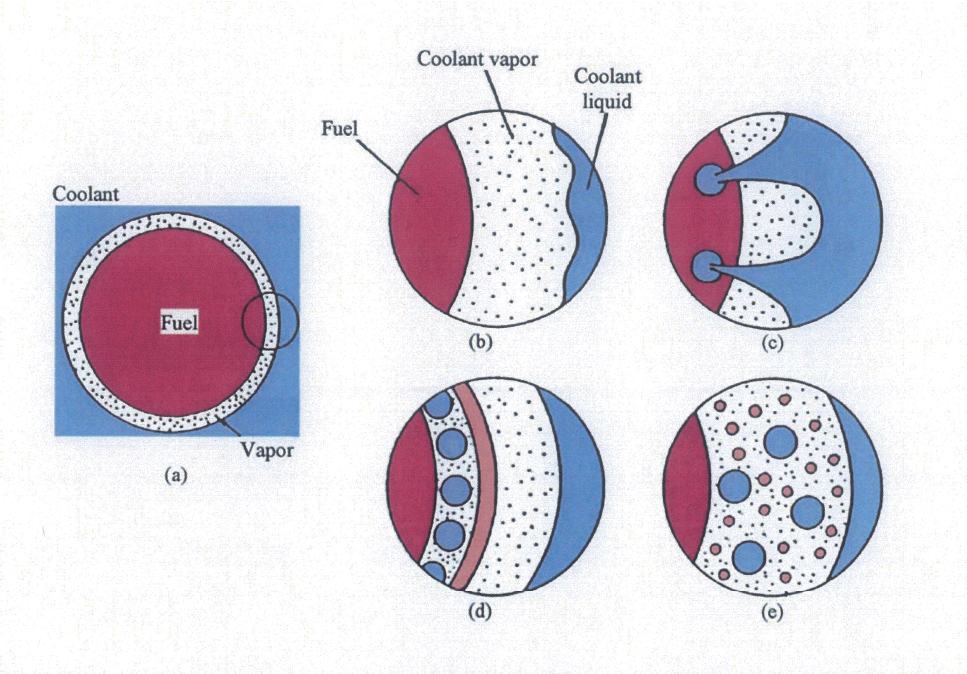

Figure 2- 1 Conceptual diagram of fine fragmentation model in the TEXAS-V code [Reference 38]

3.0 IN-VESSEL STEAM EXPLOSION ANALYSIS METHODOLOGY FOR APR1400

3.1. Introduction

In this chapter, the APR1400 design specific analysis for the evaluation of in-vessel steam explosion risk will be discussed. The analysis consists of determination of initial and boundary conditions for the in-vessel steam explosions, the structure analysis for the APR1400 RPV against the explosion loading, sensitivity analysis for key parameters that vary with the consideration of severe accident scenarios, measures and progression. Finally, the analysis results will be discussed to evaluate the IVSE risk in the APR1400 design.

3.2. Initial and Boundary Conditions

In the IVSE analysis, the complex internal structure of RPV is not considered and assumed to be divided by two regions; the molten corium region in the core region and the residual water filled in the lower plenum. This assumption is considered conservative since the complex internal structure disrupts a corium flow path and provides steam explosion triggering source, causing pre-mature steam explosion. In addition, it is assumed that corium jet is introduced at the center of the RPV and steam explosion is triggered by the bottom contact of the corium jet. This assumption also provides additional conservatism on the analysis of IVSE. The summary of the initial and boundary conditions for the TEXAS-V analysis is shown in Table 3-2. The following sub-sections describe the rationales for the selection of the quantities of the key parameters.

3.2.1. Corium Characteristics

Corium composition and thermal properties: The reference corium composition 90%UO_2-10%ZrO_2 with its thermal and transport properties as shown in Table 3-1 is chosen. Table 3-1 indicates also the properties of corium composition of 80%UO_2-20%ZrO_2 that often used in experiments that most of thermo-physical properties are similar and no significant effects of those difference on the steam explosion energetics.

Corium temperature: The base case corium temperature of 3000 K is selected. This corium temperature corresponds to the superheat of 150 K. The corium temperatures at the vessel failure are estimated by considering the results of the MAAP analysis [Reference 32], the SCDAP/RELAP 5 analysis [Reference 31] and compared with other reactor case analyses such as SERENA-I reactor application [Reference 5], AP1000 analysis [Reference 19], Japanese LWR application [Reference 15, 21].

For the oxidic layer of the corium, most of reactor case analyses used the corium temperature considering the melt superheat of 150 K. Since the oxidic layer corium temperature of 3150 K was used in AP1000 as a conservatively bounding case, sensitivity analyses for the corium temperature up to 3150 K is performed.

Corium jet diameter: The base case corium jet diameter of 0.3 m was chosen. In the in-vessel conditions, it is not feasible to consider the large diameter expected in the ex-vessel case where the RPV failure may create a major release of melt that accounts a large corium jet diameter such as 0.5m or more. In addition, it has a possibility to have multiple jets relocated from the core locations to the lower plenum. In this situation, each jet could be much thinner than one for the single jet case.

For the multi-jet case, a total of 24 jets with a diameter of 0.05 m was considered for testing the effect of multi-jet on the IVSE energetics.

Corium jet velocity: The corium jet velocity of 3 m/s is selected for the base case analysis. For the in-vessel scenario, it is not expected that corium jet is accelerated by any additional forces but by gravity.

3.2.2. Coolant Characteristics

RPV ambient pressure: The RPV pressure of 0.5 MPa is considered for the base case analysis. In general, since the effect of the ambient pressure has little effect on the steam explosion energetics, the sensitivity ranges of this parameter is not considered.

Water level and free-fall height: The depth of water level of 2.4 m is determined by the consideration that water is completely filled in the lower plenum of RPV. The free-fall height of 0.1 m is also selected by considering the distance between the core supporting plate and the water surface level.

Water temperature: Water temperature in RPV is assumed to be near saturation with the subcooling of 5 K.

3.3. TEXAS-V Modeling

3.3.1. Model Nodalization

The plant geometry of APR1400 for the TEXAS-V analysis is shown in Figure 3-1(a). The computational nodalization of the TEXAS code for the RPV is built as shown in Figure 3-1(b). The first nodalization group that represents the coolant RPV has 24 nodes that have the thickness of 0.1 m and the location of corium introduction is at 2.5m. At the bottom of the nodes, trigger cell is located to provide the trigger pressure to initiate the explosion process.

3.3.2. Model Parameters

In the TEXAS-V code, number of steam explosion model parameters, which influence the code performance and the calculation result are needed to be determined. The parameters include the jet breakup model, fine fragmentation model etc. Table 3-3 summarizes the selected parameters for the analysis. The present selections of the model parameters were intensively tested and validated during the reactor case exercise performed in the OECD/NEA SERENA-I project [Reference 5].

3.3.2.1. Melt Jet and Droplet Breakup Models for Mixing

TEXAS-V models the melt jet breakup by calculating the “blob” local relative velocity and then applying mechanistic models governed by fluid instabilities. Theoretically such a jet breakup modeling is quite complex and not well understood. Corradini and co-workers [Reference 33] have reviewed the various models for jet breakup and associated nozzle flow and categorized four mechanisms that are operative during jet breakup:

- Long-wavelength breakup of the jet as it leaves the nozzles producing discrete masses (blobs);
- Breakup of the jet along the jet column length due to Kelvin-Helmholtz (KH) instabilities;
- Breakup at the leading edge due to Boundary Layer Stripping (BLS); and
- Breakup of discrete liquid masses and the jet leading-edge by Rayleigh-Taylor instabilities.

The first form of breakup is difficult to mechanistically model, but it assists in determining the discretization of the jet as it issues forth from the nozzle. This is an active area of research, and currently TEXAS-V allows the user to fix the initial number of discrete masses at the leading edge of the jet pour (parameter NBREAK [Reference 41]). For the analysis of the OECD-CSNI standard problem (ISP-39), which is patterned after FARO L-14, the TEXAS-V analysis used NBREAK = 2 to match test results. The FARO tests were scaled to examine large jet pours of 100-500 kg/s and thus be prototypical of what may occur in a severe accident for similar size gravity jet pouring events. Similarly, for these steam explosion analyses, we have used the same logic and have assumed NBREAK = 2.

The next two forms of breakup have been modeled by TEXAS-V [Reference 41]. However, the researchers have consistently urged caution in the use of these models, since the KH and BLS mechanisms fundamentally produce very small melt particles (micron-size length scale). Such debris sizes have not been observed in actual test data. In addition, it has been found that the KH and the BLS mechanisms would be minimized by the presence of film boiling particularly when the pool is subcooled. Thus, although modeled, these breakup mechanisms have a negligible effect on jet breakup.

The final form of breakup, via Rayleigh-Taylor instabilities (RTI), is operative throughout the jet pouring process; i.e., at the jet leading-edge for discrete masses formed from the jet and for subsequent melt particles that are produced by any breakup mechanism. The work by Chu [Reference 33] developed the model that is used in TEXAS-V.

The key constitutive relation in TEXAS is this hydrodynamic fragmentation model, designated as the RTI jet breakup mechanism. This model was developed by Chu based on Pilch's original concept of a multi-step fragmentation theory for liquid particles. The model considers the fuel particles to be deformed and dynamically fragmented into a discrete number of particles from their initial diameter to smaller diameters. The fragmentation mechanism assumed in the model is Rayleigh-Taylor instabilities. The shear forces caused by the parallel velocity (e.g., Kelvin-Helmholtz instabilities and boundary layer stripping) are neglected because of their limited effects with a vapor film present and with subcooling.

The final part of the jet breakup model that needs to be explained is that the whole jet is not available for breakup by this RTI mechanism, since it is coherent and is not made up of discrete masses. Thus, after the leading edge begins to breakup with its discrete masses (blobs), any subsequent melt jet breakup can only occur when the jet overtakes and passes these discrete

masses. Lagrangian modelling continually takes account of the relative position of each discrete blob and will only allow further RTI breakup after the jet leading edge “blob” passes the other particles.

For the jet breakup model, two parameters, IENTRY and IENTRY2 with the values of 1 and 0 for both parameters, respectively, represent the jet breakup phenomena in which the stream of particles is treated as a coherent jet and the trailing edge model is the main particle break-up mechanism. In the trailing edge model, a number of independent leading particles are broken up first and the subsequent breakup occurs when the upstream particles become free and leading edge particles.

3.3.2.2. Melt Jet and Droplet Breakup Models for the Explosion

Given the triggering of an energetic FCI (or vapor explosion) by an external pressure pulse or film boiling collapse, the fuel is rapidly fragmented into fine particles (100 microns or less) due to local hydrodynamic and thermally driven instabilities. Tang and co-workers modified the original TEXAS model for fuel-coolant mixing and developed a rapid fuel fragmentation model for the explosive propagation phase of the FCI. This thermal fragmentation rate model for the fuel during this explosive propagation phase is a semi-empirical formulation based on the concept of vapor film boiling collapse and coolant jet impingement on the fuel surface to model single droplet FCI experiments. The fuel mass fragmentation rate, m_{fr}, for a specific Lagrangian ‘master particle’ is given by the expression:

$$\dot{m}_{fr} = 6C_{fr}m_p\left(\frac{P - P_{th}}{\rho_f D_p^2}\right)^{0.5} F(\alpha)g(\tau) \qquad \text{(Eq. 3.1)}$$

The constant, C_{fr}, is estimated by past theoretical work and was empirically determined by analysis of the KROTOS tests to be between 0.001 - 0.002. We use 0.002 for this constant in this analysis.

The factor, *F*, is a binary variable (1 or 0) that goes from 1 to 0 when the fuel fragmentation ceases (as the void fraction becomes large enough to become the continuous phase, fragmentation stops). This is considered a conservative value since fuel solidification effects are not considered. This fragmentation time was empirically found to vary from 0.5 to 2.0 milliseconds for good agreement with all of the KROTOS initial tests. KROTOS tests indicated that 2.0 ms was a bounding value for its one-dimensional geometry. The physical significance of this fragmentation time originates from the time it takes the explosion shock wave to propagate to the nearest free-surface, thus beginning to relieve the explosion pressure to the surroundings; i.e., the acoustic relief time. This is also correlated with the increase of the void fraction in the fuel-coolant mixture following the rapid fragmentation and the subsequent coolant vaporization. This corresponds to a void fraction of about 30 – 40 % based on analyses.

3.4. Evaluation of Dynamic Loads of IVSE – Base Case

3.4.1. Mixing Phase of IVSE

Figure 3-2 (a) illustrate the corium jet penetration during the mixing phase of the base case. The corium reached to the bottom of the RPV about 0.7 s. The penetration velocity profile shows the typical corium penetration behavior in TEXAS where the corium jet is injected with the initial velocity

and rapidly decelerated where the initial jet break-up occurs and start accelerating again. The jet break-up phenomena in the analysis can also be observed in Figure 3-2 (b) that shows the axial distribution of void and fragmented melt fractions.

Figures 3.3 and 3.4 show the void and fragmented melt fraction estimated all the axial nodes, respectively. The stacked plots for the void and fragmented melt fractions can also be found in Figure 3-5. The void fractions at all nodes in a single plot format that helps comparing the magnitudes of data while the stacked format plot in Figure 3-5 provides the progression of void fractions along with the corium penetration. The maximum void fraction reached up to 80% at the upper location where the jet velocity was rapidly decelerated. However, the void fractions in the lower region were very low although the corium jet fragmented as shown in Figure 3-5. Therefore, it is expected that steam explosion occurs due to the bottom triggering and propagates upward, triggering subsequent explosions. However, due to the large volume of void at the upper location, shock pressure will be diminished. It is also noted that the near saturation water temperature is responsible for this large volume of steam generation.

3.4.2. Explosion Phase of IVSE

Figures 3.6 and 3.9(a) show the steam explosion pressure profiles in terms of the explosion time. The maximum pressure and impulse of 37.5 MPa and 62.3 kPa-s, respectively. the steam explosion pressures along the axial direction in terms of the explosion time. Figures suggest that the explosion pressure reached its maximum of 37.5 MPa. The pressure profiles show the typical shock characteristics as the rapid build-up of pressure front and a long tail with respect to time. The explosion pressure front traveled with velocity of 1400~1500 m/s up to the location of L7 and dissipated in the upper axial location due to the presence of a volume of steam as shown in the mixing phase.

Figures 3.7 and 3.9 (b) shows the void fraction profiles during the explosion phase. The lower part of the lower head where steam explosion was triggered builds up their steam due to the explosion near 100% during the period the explosion phase. The upper region where the steam generated in the mixing phase shows the rapid condensation during the explosion phase period, 20 ms.

The impulse asserted to the surrounding structure was estimated by the integration of the explosion shock pressure during the explosion period. The evaluated impulses at each node are shown in Figure 3-8(a). The impulse at the node of cavity floor reached 62.3 kPa-s. The maximum possible energetics of steam explosion in this case estimated by the 1-D TEXAS-V analysis will travel (and be attenuated) to the surrounding internal structure in RPV. However, in this analysis to evaluate the RPV structure response against the explosion loading, the maximum pressure and impulse are assumed to be applied on the inner RPV wall. Therefore, no shock attenuation is considered.

Figures 3.8(b), (c) and (d) show more insights of the explosion phase of the steam explosions in RPV that include the energy partitioning, the coolant kinetic energy and the conversion ratio history during the explosion phase. In particular, the conversion ratio of the steam explosion reaches its maximum of near 1.0% after the triggering of explosion.

3.4.3. Sensitivity Study: Multi-Jet Effect

For the sensitivity study, three additional cases for investigating the effect of multi-jet configuration

are studied. The cases includes (a) multi-jet case with the single jet diameter of 0.05m and 36 jets, (b) multi-jet case with the single jet diameter of 0.1 m and 9 jets and (c) the SERENA-I configuration with the single jet diameter of 0.08m and 24 jets as shown in Figure 3-10.

Table 3-4 summarized the results of the analyses and compared with the base case. The cases (a) and (b) were design to keep the equivalent diameters for both cases equal to one in the base-case single jet analysis, 0.3m. However, the equivalent diameter of the case (c) was larger.

The peak pressures estimated ranges from 50 to 87 MPa. The SERENA case shows the maximum peak among the cases. However, the maximum impulse was observed in the case (a), estimated near 100 kPa-s. For the multi-jet cases, the total mixing times are longer than one for the base case due to the steam generation induced drag forces. It is also observed that the mixing time increases when the number of jet increases. The maximum impulses are also increases with the number of jets. It can be explain that in the case of multi-jet the longer mixing time allows more melt jets to be fragmented. It is possible in TEXAS-V analysis because TEXAS was set to provide an optimal mixing conditions for the given jet-water configuration to maximize the energetics. However, in the real situation, the multi-jet configuration may produce more a steam rich mixing zone caused by (a) more fragmentation of jets and (b) limited radial dispersion of fragmented melts and thus result lower energetics. In this sensitivity analysis, it is now expected that the ranges of the maximum impulses that impose on the RPV inner wall will be approximately 60-100 kPa-s.

3.5. Introduction of RPV Structure Analysis

3.5.1. Design Criteria

The design criteria used in the ARP1400 reactor vessel [Reference 25] are based on the ASME Boiler & Pressure Vessel Design Code Section III NR-3200 [Reference 42]. Detailed stress analysis for all of major components would be prepared to satisfy stress limit of NB-3220 and NB-3230 when load of NB-3110 is the main component. In this report, reactor vessel designs and stress limit are same with the design use in APR1400 reactor vessel report but stress analysis method is different.

In this study, the most conservative failure criteria suggested by Shockey who adopted the concept of ductile fracture apparatus based on void generation and growth is used. He suggested that void was generated from precipitation particle and critical strain required for void nucleus generation at 11%.

3.5.2. Dynamic Loads to RPV due to Steam Explosion

The RPV structure analysis is required to evaluate the dynamic response of RPV against the impeding IVSE pressure loadings. First, using the simplified pressure profile, the pressure and impulse criteria that cause the RPV failure will be examined. In so doing, a simplified explosion pressure profile that has a triangular pressure pulse with a given P_{max} at the center and pulse with Δt as shown in Figure 3-11 is used. In this study, the pulse with of 5ms was used.

3.6. Evaluation of RPV Structure Analysis

This part calculates the effect of dynamic pressures from a steam explosion on APR1400 reactor vessel and evaluates integrity of structure. It is hard to know where the start point of explosion and

it can cause much different result in stress analysis because it is related to applying time of dynamic pressure to wall in reactor vessel. We assume explosion happen at center of bottom head. It makes dynamic pressure apply to whole wall of the bottom head at same time. In real condition, liquid is pressure carrier and pressure damper when steam explosion happens. However, it is assumed that liquid is a pressure carrier without any attenuation. Therefore, the steam explosion pressure is applied directly to the inner wall of RPV.

For the analysis, ABAQUS 6.10 is used for the stress analysis FEM tool. To apply real time to stress analysis, the explicit mode of ABAQUS is used. Figure 3-12 shows the axisymmetric model of the RPV that the lower head is hemisphere.

ABAQUS has a large finite element library for 2-D and 3-D, cell, and solid. Figure 3-12 shows the basic dimension of geometric configuration of lower head. The lower head material is the SA508 class3 with characteristic of elastic-linear plastic including strain hardening effect. The material characteristics at 500^{o}F are as follows.

Young's modulus E = 0.27×10^{-8} psi

Poisson's ratio v = 0.3

Yield stress σ_y = 50,000 psi

Allowable stress intensity Sm = 30,000 psi

Tangent modulus ET = 0.235×10^{-6} psi

Density ρ = $0.283\,\frac{lb}{in^3}$

Figure 3-13 shows finite element model for the numerical grid that consists of four nodes elements, CAX4R, with the axi-symmetry boundary conditions. The total number of nodes is 440 and the total number of elements is 348.

Two boundary conditions should be specified in this model. Y-direction symmetry is applied at top side. X-direction symmetry is applied at left side. Y axi-symmetry is applied at model. Pressure is applied at inside and tabular data is used.

3.6.1. Results of Structure Analysis

3.6.1.1. Stress Analysis for Design Conditions

The design pressure of 17.2MPa(2,500psi) acts on the inner lower head of the APR1400 design. In the analysis the maximum stress of 165.4MPa and allowable value of 344MPa (50,000psi) have been obtained. In the case, the maximum equivalent strain is 0 % that is much less value than 11 % of allowable.

3.6.1.2. Stress Analysis for IVSE Conditions

For the analysis, the initial pressure of 0.5MPa that was assumed in the in-vessel pressure is applied on the inner lower head. Pressure increases to its maximum pressure linearly during 2.5ms and decreases to the initial pressure during additional 2.5ms. The initial vessel pressure of 0.5MPa is maintained. In this analysis, the peak explosion pressures of 25, 50, 75, 100, 125, 150 and 175 MPa have been applied to the reactor vessel to map the allowable criteria of the maximum plastic equivalent strain of the reactor vessel. The peak pressures correspond to the impulses of 62.5, 125, 187.5, 250, 312.5, 375 and 437.5 kPa-s.

Three different cases with the peak pressure of 50, 100, 150 MPa are discussed to illustrate the responds on RPV structure against explosion loadings and shown in Table 3-5. In case of the maximum pressure of 50MPa, the maximum plastic equivalent strain is 0.618% at 3.5ms. Time histories for plastic equivalent strain and von mises stress of node that show maximum plastic equivalent strain are shown in Figure 3-14. These stress and strain are increased with time and vibrate under specific maximum plastic equivalent strain.

In case of maximum pressure 100MPa, maximum plastic equivalent strain is 17.29% at 9.5ms. Time histories for plastic equivalent strain and von mises stress of node that show maximum plastic equivalent strain are shown in Figure 3-15. These stress and strain are increased with time and vibrate under specific maximum plastic equivalent strain.

In case of the maximum pressure of 150MPa, the maximum plastic equivalent strain is 61.36% at 10ms. Time histories for plastic equivalent strain and von mises stress of node that show maximum plastic equivalent strain are shown in Figure 3-16. These stress and strain are increased with time and vibrate under specific maximum plastic equivalent strain. In this study, the stress limit on the node that plastic deformation occurred was observed at about 350MPa.

Figure 3-17 show the maximum hoop strain in terms of explosion impulse. The failure criteria limit of 50% maximum hoop strain corresponds to the explosion impulse of about 400 kPa-s. For the strain based failure criteria, Figure 3.18 summarized the structure responses on the explosion impulse. It shows the the Shockey criteria of 11% is the most conservative among others. For the criteria, the APR1400 RPV design can be safely maintain its integrity up to 215 kPa-s. The analysis evaluates the effect of dynamic pressures from a steam explosion on the integrity of the APR1400 reactor vessel. The present IVSE energetics of 62.3 kPa-s shows near zero strain in the RPV, well below the failure criteria. It is concluded that no threat of the APR1400 lower head due to the in-vessel steam explosion is expected.

3.7. Summary and Conclusions

For the IVSE analysis, there are number of assumptions that contribute to the analysis conservative. Those assumptions include;

(a) Simplified internal geometry in RPV provides conservative assumptions on the corium configuration and early triggering

(b) Bottom trigger of corium jet provides the maximized corium mixing and melt participation for explosion without additional build-up for the steam before the triggering of steam explosion

(c) No explosion pressure shock attenuation from the location of IVSE to the RPV inner wall

(d) One-dimensional analysis using TEXAS-V provides the maximum explosion energetics for the given mixing condition

(e) No shock pressure attenuation from the location of explosion to the inner wall of RPV for the RPV structure analysis

(f) Shiocky's criteria is conservative among other failure criteria evaluated in this study.

Under the consideration of the conservative assumptions, the structure analysis shows that no threat of the APR1400 lower head due to the in-vessel steam explosion is expected.

Table 3- 1 : Corium Properties

TS

Table 3- 2 Initial and Boundary Conditions for the IVSE analysis with TEXAS-V

TS

Table 3- 3 The TEXAS-V model parameters selected for the analysis

TS

Table 3- 4 Sensitivity Studies for Multi-jets

TS

Table 3- 5 Summary of the results of the simplified steam explosion cases (50, 100 and 150

TS

Figure 3- 1 TEXAS-V Nodalization for the In-Vessel Steam Explosion in the APR1400 RPV